Nano Energy 68 (2020) 104326

Contents lists available at ScienceDirect

Nano Energy

journal homepage: http://www.elsevier.com/locate/nanoen

Communication

$Ge_2Sb_2Se_5$ Glass as High-capacity Promising Lithium-ion Battery Anode

Jassiel R. Rodriguez [a,*], Zhimin Qi [b], Haiyan Wang [b], Mikhail Y. Shalaginov [c], Claudia Goncalves [d], Myungkoo Kang [d], Kathleen A. Richardson [d], J. Guerrero-Sanchez [e], Ma Guadalupe Moreno-Armenta [e], Vilas G. Pol [a]

[a] Davidson School of Chemical Engineering, Purdue University, West Lafayette, IN, 47907, USA
[b] School of Materials Engineering, Purdue University, West Lafayette, IN, 47907, USA
[c] Department of Materials Science and Engineering, Massachusetts Institute of Technology, Cambridge, MA, 02139, USA
[d] College of Optics and Photonics, Department of Materials Science and Engineering, University of Central Florida, Orlando, FL, 32816, USA
[e] Centro de Nanociencias y Nanotecnología, Universidad Nacional Autónoma de México, Ensenada, BC, 22860, Mexico

ARTICLE INFO

Keywords:
Chalcogenide glass material
$Ge_2Sb_2Se_5$
Anode
High capacity
Li-ion battery

ABSTRACT

Conventional alloying and conversion Li-host anode materials have been extensively studied as high capacity lithium ion battery anodes. However, they suffer continuous volume change during each charge-discharge process, triggering the electrode pulverization and loss of their capacity upon cycling. Interestingly, investigations on glass materials as Li-host anodes are less prevalent, although their disorder structure can help to accommodate their volumetric expansion and maintain the anisotropic particle arrangement with a better distribution during Li-ion insertion and extraction. Here, we report attributes of a promising candidate chalcogenide glass material, $Ge_2Sb_2Se_5$, which exhibits a reversible high capacity of 626 mAh g^{-1} at a 0.5 C-rate, displays a capacity retention of 80% with a coulombic efficiency of >99% after 100 cycles. The resulting material performance is explained by a proposed lithiation mechanism in which lithium ions are alloyed with Se atoms at high potential, followed by the lithiation of Sb and Ge as the potential decreases during the discharge process. DFT calculation suggests an optimized glassy cell unit of $Ge_2Sb_2Se_5$ with an energy gap of 0.14 eV, proposing a possible arrangement of atoms with short range order, in which the large variation of the nearest neighbor distances in $Ge_2Sb_2Se_5$ can promote its stable anodic performance.

1. Introduction

Since its introduction in the secondary battery market (SONY ©, 1991), Li-ion batteries (LIBs) have achieved great success in a wide variety of domestic, medical, security and portable applications [1–3], due to their high power and energy density, stable performance during hundreds of charge-discharge cycles, and reasonable cost [4–7]. However, the constant increase of demand for LIBs with high Li-ion storage, stable performance and long-life cycling motivates the quest towards developing and improving high capacity Li-host anode materials [8–11]. Commonly employed graphitized carbon has been extensively used as a commercial anode, offering a moderate theoretical specific capacity of 372 mAh g^{-1} (with an experimental capacity ~330 mAh g^{-1} at moderate C-rate of C/5) through the electrochemical redox reactions: $Li + 6C \leftrightarrow LiC_6$. This capacity has been shown to be insufficient to fulfill the energy needs of our dynamic modern society [8,12].

Promising Li-host anode materials with high performance have been developed using several strategies, such as, particle size reduction [13–15], increasing the electrode conductivity [16–20], and design new architectures [21–24] or active phases [25–29], in which their physico-chemical properties can promote some interesting synergistic effects that could lead to an improvement in their electrochemical properties.

Chalcogenide materials have attracted considerable attention as Li-host anode materials [30–32], since they can reach high levels of Li-ion storage through conversion and alloying [33–36] electrochemical reactions. Glassy materials possess unique and favorable physical-chemical, mechanical and textural properties that allow them to suppress huge volumetric changes during the charge-discharge processes, avoiding the electrode pulverization, maintaining a good connectivity and electron mobility through the negative electrode [37,38]. Therefore, chalcogenide glass materials have exhibited high Li-ion

* Corresponding author.
E-mail address: rodri571@purdue.edu (J.R. Rodriguez).

https://doi.org/10.1016/j.nanoen.2019.104326
Received 6 August 2019; Received in revised form 6 November 2019; Accepted 24 November 2019
Available online 27 November 2019

mobility in LIB systems [39–42] with better or special physical-chemical properties (i.e., ionic conductivity, electrochemical and mechanical stability) in comparison to their single or poly-crystalline counterparts [34,43–46]. These characteristics made chalcogenide glasses as interesting materials with certain potential as Li-ion host anode for LIB or beyond Li-ion applications.

Here, we report electrochemical performance of a promising amorphous Li-host $Ge_2Sb_2Se_5$ (GSSe) anode material prepared by using the conventional melt-quenching (M-Q) technique (Scheme 1). Electrochemical results demonstrated that multi-component Ge, Sb and Se-containing material exhibits a high theoretical specific capacity of ~848 mAh g^{-1} (around 2 times higher than graphite), and exceeds that shown in other systems based on ~22 at.% of Ge (1600 mAh g^{-1}) [47], ~22 at.% of Sb (660 mAh g^{-1}) [48] and ~56 at.% of Se (678 mAh g^{-1}) [49]. It was found that the combination of high capacity Li-host materials in a previously unexplored amorphous network structure offers promising electrochemical performance.

2. Result and discussion

Fig. 1a shows a DSC thermogram with an endotherm dip at 265 °C with a glass transition temperature (T_g) of 245 °C. The as-quenched material illustrates evidence of quenched-in nuclei as illustrated in the onset of an exothermic crystallization peak (T_x) near 300 °C. The temperature interval ΔT between T_g and the onset crystallization temperature (T_x) is considered as an indicator of glass stability, where $\Delta T = T_x - T_g$. While the exotherm in Fig. 1a suggests possible crystallization, no peaks are observed in Fig. 1b which depicts the XRD pattern for powdered GSSe material, portraying two broad diffraction humps featuring amorphous phase. The lack of distinct diffraction peaks in the XRD patterns confirm the as-melted material is amorphous. Also, the glassy GSSe material with a short order arrangement was modelled following Sun et al. [53] procedure. The disordered GSSe supercell contains Ge and Sb vacancies randomly generated, and the relaxed GSSe glass model is composed of 324 atoms (see Fig. 1c and S1). After full optimization of the disordered GSSe atomic network, it is clear the obtention of a glass behavior since the nearest neighbor distances have large variations for almost all atoms. The main Ge–Sb, Ge–Ge, Ge–Se, Se–Sb, Se–Se and Sb–Sb bond lengths are depicted in Table S1. The density of states of the glassy GSSe is shown in Fig. S2, it presents a semiconductor behavior with an energy gap of 0.14 eV. While its valence band maximum (VBM) is mostly dominated by Se-p states, the conduction band minimum (CBM) is contributed by the hybridization of Ge-p, Sb-p and Se-p states.

A topographic image of GSSe particles acquired by SEM reveals the presence of agglomerated particles with nanometric size and random shape (see Fig. 1d). Additional topographic images (see Fig. S3) depict a mixture of pristine GSSe sample and carbon materials. LR-TEM micrograph (Fig. 1e) clearly shows a single GSSe nanoparticle of a thin laminal shape. HR-TEM micrograph (Fig. 1f) demonstrates no obvious crystallographic lattice fringes, indicating the amorphous nature of GSSe particles. The selected area electron diffraction (SAED, Fig. 1g) pattern confirms the characteristic anisotropic atomic arrangement of GSSe particles. Interestingly, Fig. S4 also reveals the existence of both amorphous and polycrystalline GSSe particles, suggesting the formation of some small size crystallites during synthesis process. Furthermore, the EDX mapping data in Fig. 1h-k confirms the presence of Ge (red), Sb (blue), and Se (green), similar to EDS information obtained using SEM in Fig. S3, in the GSSe nanoparticle.

Fig. 2a shows the cyclic voltammetry (CV) information obtained from glassy GSSe electrode as Li-host anode, which was acquired at 0.2 mV s^{-1} between 0.01 and 3.0 V *vs* Li/Li^+. During the first cathodic scan, the irreversible broad peaks at about 1.66, 1.21, 0.52 and 0.01 V *vs* Li/Li^+ were induced by the solid electrolyte interphase (SEI) layer formation, conversion and alloying reactions that occur between GSSe glass chalcogenide and Li. The well-overlapped cathodic peaks on the subsequent CV curves are associated with the lithiation reaction: (1) at high potential, 1.66 V *vs* Li/Li^+, $Se + 2Li \rightarrow Li_2Se$ [54]; (2) at 1.21 V *vs* Li/Li^+, $GeSe_2 + 2Li \rightarrow Ge + GeSe + Li_2Se$ [55] or $Sb_2Se_3 + 6Li \rightarrow 2Sb + 3Li_2Se$ [35]; (3) at 0.52 V *vs* Li/Li^+, $Sb + 3Li \rightarrow Li_3Sb$ [56] or $GeSe + 2Li \rightarrow Ge + Li_2Se$ [55]; (4) at low potential, 0.01 V *vs* Li/Li^+, $Ge + 4.4Li \rightarrow Li_{4.4}Ge$ [47,55,57], revealing a stable electrochemistry. During the positive scans appeared some anodic peaks associated to the delithiation reaction: (1) at 0.56 V *vs* Li/Li^+, $Li_{4.4}Ge \rightarrow Ge + 4.4Li$; (2) at 1.09 V *vs* Li/Li^+, $Li_3Sb \rightarrow Sb + 3Li$; (3) at 1.64 V *vs* Li/Li^+, $Li_2Se + Sb \rightarrow Li_xSb_2Se_3$ [35]; at 2.2 V *vs* Li/Li^+, $Li_xSb_2Se_3 \rightarrow Sb_2Se_3 + xLi$ [35].

The cyclability and rate capability of GSSe glass chalcogenide particles were studied by galvanostatic charge-discharge measurements, where capacities were calculated based on the mass of GSSe. Fig. 2b shows the charge-discharge profiles of the GSSe anode for cycle 1st, 2nd and 100th acquired at a C-rate of 0.5C, between an electrochemical window from 0.01 to 3.0 V *vs* Li/Li^+. The GSSe anode delivered an initial specific discharge capacity of around 1611 mAh g^{-1} at 0.05 C-rate. This value of capacity is higher than GSSe's theoretical specific capacity (848 mAh g^{-1}) because the SEI layer is formed during the 1st discharge cycle of the anodic electrode in the half cell configuration, which is clearly observed in Fig. S5. The cross-section SEM images depict that the cycled GSSe electrode suffers an expansion of 26% (from 19 to 24 μm), indicating that the amorphous arrangement of the glassy GSSe chalcogenide partially suppresses the volume expansion of Ge, Sb and Se upon cycling. However, the active glass material gives a high specific discharge capacity of about 626 mAh g^{-1} at 0.5 C-rate with a capacity retention of 80% after the second cycle and a coulombic efficiency of 99.2% after 100 cycles. Fig. 2c displays the cycle performance of GSSe anode, which shows a stable behavior with a continuous decay of capacity during few cycles, reaching a reversible discharge capacity of 626 mAh g^{-1} after 100 cycles, that continuous loss of capacity could be associated with the disconnection of the active particles from the electrode as a result of the electrode pulverization [58], which can generate mechanical stress, cracks and fractures inside the anodic electrode. Dependence of dQ dV^{-1} vs potential (see Fig. 2d) reveals that for the cycle 5th, 50th and 100th, Se is getting inactive as the reaction proceeds. At the same time, more Ge participates during the electrochemical redox reaction of lithium, which leads to a stable performance without a significant capacity decay after 50 cycles. During this process the Se inactivation could be related to its partial dissociation inside the electrolyte by the formation of soluble polyselenides species [35], as Fig. S6 displays the presence of Se on the PP separator and Li counter electrode, confirmed by EDS analysis. Meanwhile, the increment of Ge activation could result from the electrode pulverization, allowing the participation of Ge in the core of GSSe

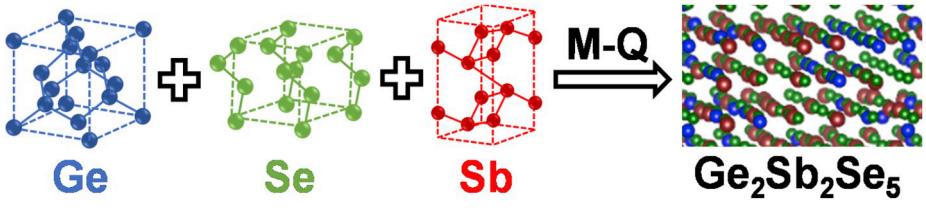

Scheme 1. Preparation of glassy GSSe powder from crystalline sources via melt-quenching.

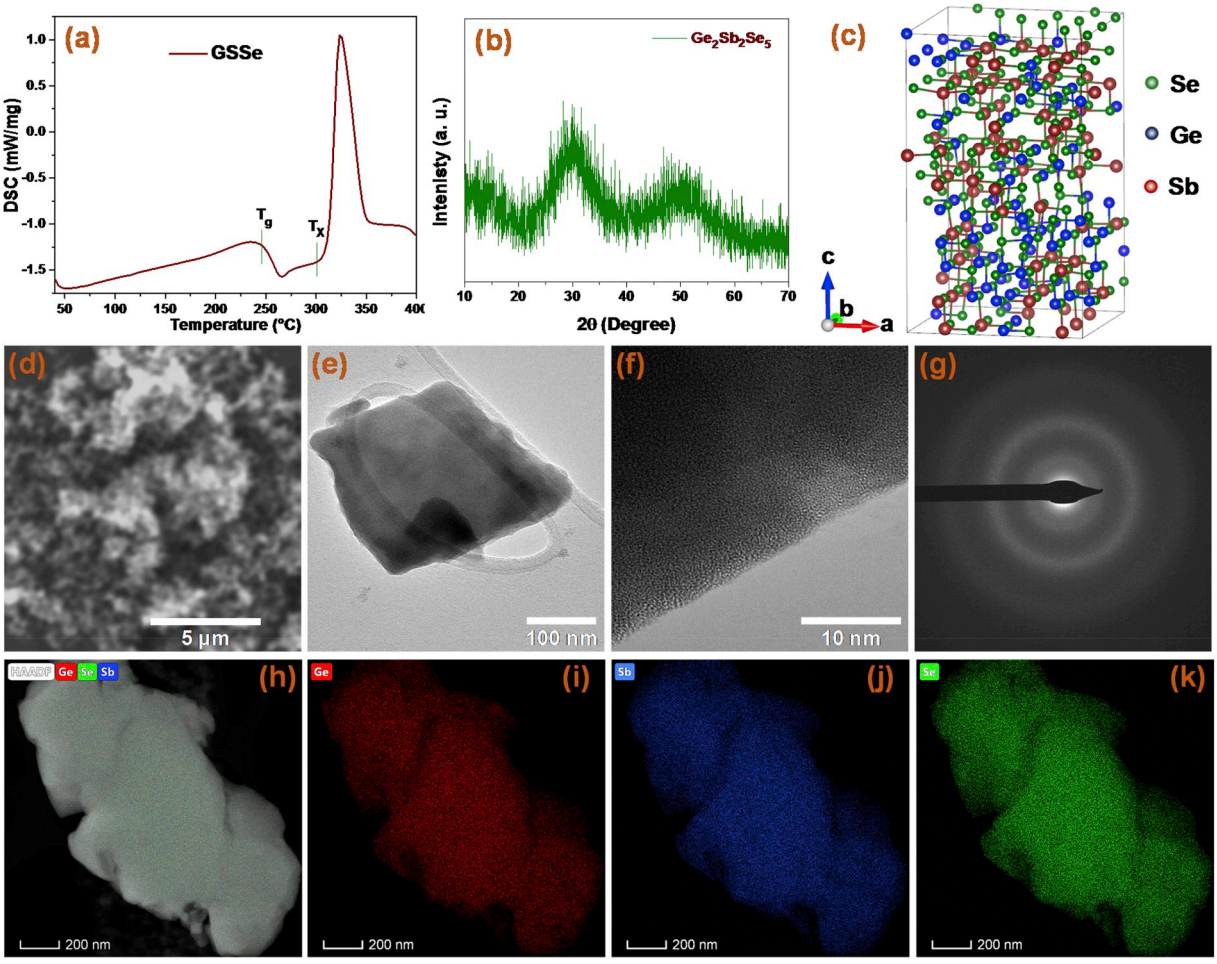

Fig. 1. Characterization of amorphous GSSe powder: (a) DSC spectrum of as-melted GSSe glass chalcogenide; (b) X-ray diffraction pattern of GSSe glass powder; (c) 3D unit cell of glassy GSSe depicting simulated atomic arrangement, Se (green), Ge (blue) and Sb (red); (d) SEM image of agglomerated microparticles; (e) low- and (f) high-resolution TEM micrographs of an individual GSSe nanoparticle; (g) selected-area electron diffraction pattern; (h)–(k) EDS analysis of a GSSe nanoparticle, Ge (red), Sb (blue), and Se (green).

microparticles. Fig. S7 demonstrates the presence of rich- and poor-Se regions on the electrochemically active material after cycling, which keeps its anisotropic arrangement, but its morphology and elemental composition changed upon cycling (TEM and EDS studies in Figs. S7 and S8). Fig. 2e presents Nyquist plot of cycled glassy electrode, in which the cycled one contains two overlapped semicircles at high and low frequencies, related to the electrode/electrolyte interface layer (6 Ω) and the charge transfer (14 Ω) resistances, respectively, indicating the formation of a stable SEI layer on the glassy GSSe anode. Also, a linear tail indicates an existence of semi-infinite linear Li-ion diffusion or Warburg impedance [3], with a Li-ion diffusion coefficient value of $\sim 1.2 \times 10^{-14}$ cm^2 s^{-1} for the amorphous GSSe chalcogenide.

The rate capability of the glassy GSSe chalcogenide anode was studied at different C-rate values during 10 D-C cycles, see Fig. 2f. The glass material exhibits an average of specific discharge capacities of 925, 849, 755, 638, 554 mAh g^{-1}, and back to 798 mAh g^{-1} at C-rate of 0.05, 0.1, 0.2, 0.5, 1 C, and back to 0.1C, respectively. The glassy GSSe anode displays a high C-rate capability, delivering 554 mAh g^{-1} capacity at 1 C-rate, which is about two times higher than traditional graphitic anodes (~300 mAh g^{-1} at 0.2C). Glassy GSSe anode exhibited high reversible capacity, good rate capability with stable behavior, such performance could be related to a synergistic effect between Ge and Sb selenides during the conversion and alloying redox reactions. As shown in Fig. S9, the electrode of Sb gives a long cycle stability but lower capacity than the Ge electrode during the initial 50 D-C cycles. Additionally, the electrochemical behavior of the GSSe electrode was evaluated between 0.01 and 1.5 V *vs* Li/Li^+ (Fig. S11). Under this condition, the active material delivers a high specific capacity of 503 mAh g^{-1} at 0.5 C-rate after 100 cycles that is less than the delivered capacity of 626 mAh g^{-1} at 0.5 C-rate (between 0.01 and 3.0 V *vs* Li/Li^+). This is due to the suppression of selenium redox reactions after the formation of Li_2Se, which leads to increase in the solid-electrolyte interface and charge transfer resistance by 3 times each one. However, the Ge and Sb reactions deliver a stable redox performance as the physical-chemical and textural properties of glassy $Ge_2Sb_2Se_5$ allows a good connectivity between the electroactive particles, carbon additive and binder, producing a promising anodic electrode for next generation Li-ion batteries.

3. Conclusion

In summary, this is the first report, where glassy $Ge_2Sb_2Se_5$ particles are used as Li-host anode material, delivering a promising reversible high specific discharge capacity of 626 mAh g^{-1} at a C-rate of 0.5C with 99.2% coulombic efficiency after 100 cycles and with high rate capabilities, in which the glass chalcogenide electrode reaches 554 mAh g^{-1} capacity at 1 C-rate. This novel, electrochemically active GSSe glass chalcogenide anode material enables a new approach to design high-capacity and stable Li-host anode materials for the next generation of rechargeable batteries.

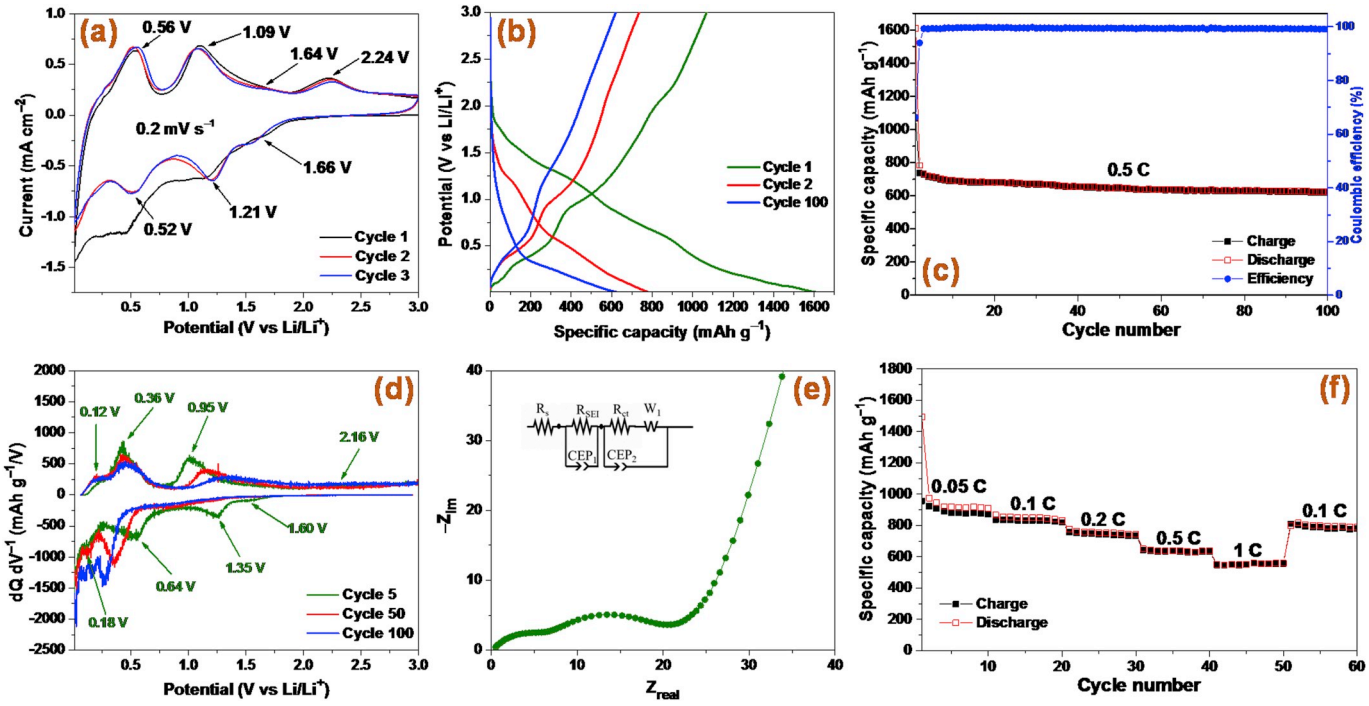

Fig. 2. Electrochemical properties of glassy GSSe anodes: (a) cyclic voltammetry at 0.2 mV s^{-1}; (b) charge-discharge profiles; (c) cycle performance at 0.5 C-rate; (d) dQ dV^{-1} plot; (e) electrochemical impedance spectroscopy data after cycling with its corresponding circuit fitting; and (f) rate capability. C-rate was calculated based on 848 mAh g^{-1} at 1 C.

4. Experimental section

4.1. Material preparation

$Ge_2Sb_2Se_5$ (GSSe) chalcogenide glass was prepared by a conventional melt-quenching technique, using high purity (metals basis, 5 N) raw materials (Ge, Sb, Se) in the exact stoichiometry. The weighed batch was loaded into cleaned fused quartz tube and sealed under vacuum using a methane–oxygen torch to form a sealed ampoule. The tube was placed into a rocking furnace at 850 °C, to homogenize the melt. After overnight rocking at elevated temperature, the furnace was then cooled to the quench temperature, $T_Q = 750$ °C, and quenched using compressed air flow over the ampoule. The batch was then annealed for 2 h ($T = 230$ °C) in order to remove residual stress, cooled down slowly to room temperature, and removed from the ampoule for subsequent characterization.

4.2. Characterizations

Characteristic temperatures of glass transition (T_g) and crystallization (T_x) were determined by differential scanning calorimetry (Netzsch DSC 204 F1 Phoenix). During this procedure small powder samples about 20 mg were loaded into sealed aluminum pans. Then, the samples were heated at a rate of 10 °C min^{-1} from 25 °C to 400 °C. To confirm the amorphous nature of the prepared materials, GSSe particles were analyzed using powder X-ray diffraction (XRD) technique in a Rigaku diffractometer with Bragg-Brentano. Subsequently, the topographic information of the GSSe material was examined by using scanning electron microscopy (JEOL NeoScope JCM6000). A microstructural analysis was performed with transmission electron microscopy (FEI Talos) at 200 kV in bright and dark field modes. Additionally, the chemical composition was identified using energy dispersive X-ray (EDX) spectroscopy.

4.3. DFT calculation

Ab-initio total energy calculations to simulate the glassy $Ge_2Sb_2Se_5$ structure were carried out using Vienna ab-initio simulation package (VASP) [50]. In order to treat the exchange and correlation effects, we have used the generalized gradient approximation as stated by the Perdew-Burke-Ernzerhof parametrization [51]. Core electron states were represented by the projector augmented-wave method (PAW) [52]. For structural optimizations, the electronic states were expanded in a plane-wave basis set with cutoff energy of 408 eV. The electronic states were evaluated in a gamma centered and equally spaced k-points on a grid of $2 \times 2 \times 1$. We evaluated the density of states and projected density of states by utilizing a denser k-points grid of $8 \times 8 \times 3$.

4.4. Electrochemical evaluation

The electrochemical performance of GSSe particles as Li-host anode material was studied using cyclic voltammetry (CV) and charge-discharge cycling. First, GSSe powder was mixed with graphene, Super P carbon, and polyvinylidene fluoride (PVdF) in a mass ratio of 70:10:10:10 in NMP solvent. The resultant slurry was casted on a Cu foil, followed by solvent evaporation in vacuum. The film was punched out to obtain a working electrode with a diameter of 12 mm and active mass of 2.5 mg. The electrochemical analysis was carried out in 2032 coin-type cells, using Li foil as a counter electrode, Celgard™ 2500 discs as separator, and 1.0 M $LiPF_6$ in ethylene carbonate (EC) and diethyl carbonate (DEC) (1:1 volume ratio) as electrolyte.

The Li-ion diffusion coefficient of the GSSe anode was calculated according to next equation:

$$D = \frac{0.5R^2T^2}{S^2n^4F^4c^2\sigma^2} \quad \text{(i)}$$

Where, D is the diffusion coefficient (cm^2 s^{-1}); R is the universal gas constant (8.314 J $mol^{-1}K^{-1}$); T is the absolute temperature (K); S is the surface area of the electrode (1.27 cm^2); n is the charge transfer number; F is the Faraday's constant (96486 C mol^{-1}); c is the lithium ion concentration (0.047 mol cm^{-3}); and σ is Warburg factor that can be calculated from the slope of Z′ vs $\omega^{-1/2}$ graph (Fig. S12).

Declaration of competing interest

The authors declare that they have no known competing financial interests or personal relationships that could have appeared to influence the work reported in this paper.

Acknowledgment

Authors thank to Professor Hu from department of materials science and engineering, MIT for his recommendations. This work was supported in part by CONACYT-SENER project No. 274314 and U.S. Office of Naval Research (ONR, N00014-16-1-2465). G. Moreno and J. Guerrero thank DGAPA-UNAM for the financial support, projects IN114817-3 and LANCAD-UNAM-DGTIC-150.

Appendix A. Supplementary data

Supplementary data to this article can be found online at https://doi.org/10.1016/j.nanoen.2019.104326.

References

[1] X.B. Cheng, R. Zhang, C.Z. Zhao, Q. Zhang, Toward safe lithium metal anode in rechargeable batteries: a review, Chem. Rev. 117 (2017) 10403–10473, https://doi.org/10.1021/acs.chemrev.7b00115.
[2] N. Nitta, F. Wu, J.T. Lee, G. Yushin, Li-ion battery materials: present and future, Mater. Today 18 (2015) 252–264, https://doi.org/10.1016/j.mattod.2014.10.040.
[3] J. Tang, V. Etacheri, V.G. Pol, Wild fungus derived carbon fibers and hybrids as anodes for lithium-ion batteries, ACS Sustain. Chem. Eng. 4 (2016) 2624–2631, https://doi.org/10.1021/acssuschemeng.6b00114.
[4] J.W. Choi, D. Aurbach, Promise and reality of post-lithium-ion batteries with high energy densities, Nat. Rev. Mater. 1 (2016) 1–16, https://doi.org/10.1038/natrevmats.2016.13.
[5] A. Manthiram, An outlook on lithium ion battery Technology, ACS Cent. Sci. 3 (2017) 1063–1069, https://doi.org/10.1021/acscentsci.7b00288.
[6] Y. Li, H. Zhang, Y. Chen, Z. Shi, X. Cao, Z. Guo, P.K. Shen, Nitrogen-Doped carbon-encapsulated SnO2@Sn nanoparticles uniformly grafted on three-dimensional graphene-like networks as anode for high-performance lithium-ion batteries, ACS Appl. Mater. Interfaces 8 (2016) 197–207, https://doi.org/10.1021/acsami.5b08340.
[7] H. Ying, S. Zhang, Z. Meng, Z. Sun, W.-Q. Han, Ultrasmall Sn nanodots embedded inside N-doped carbon microcages as high-performance lithium and sodium ion battery anodes, J. Mater. Chem. A. 5 (2017) 8334–8342, https://doi.org/10.1039/C7TA01480E.
[8] D.M. Piper, J.J. Travis, M. Young, S.B. Son, S.C. Kim, K.H. Oh, S.M. George, C. Ban, S.H. Lee, Reversible high-capacity Si nanocomposite anodes for lithium-ion batteries enabled by molecular layer deposition, Adv. Mater. 26 (2014) 1596–1601, https://doi.org/10.1002/adma.201304714.
[9] E. Allcorn, A. Manthiram, FeSb2-Al2O3-C nanocomposite anodes for lithium-ion batteries, ACS Appl. Mater. Interfaces 6 (2014) 10886–10891, https://doi.org/10.1021/am500448f.
[10] J.R. Rodriguez, C. Belman-rodriguez, S.A. Aguila, Y. Zhang, H. Liu, V.G. Pol, Bismuth Germanate (Bi4Ge3O12), a Promising High-Capacity Lithium-Ion Battery Anode, 2018, pp. 11483–11486, https://doi.org/10.1039/c8cc05861j.
[11] R.A. Adams, V.G. Pol, A. Varma, Tailored solution combustion synthesis of high performance ZnCo2O4 anode materials for lithium-ion batteries, Ind. Eng. Chem. Res. 56 (2017) 7173–7183, https://doi.org/10.1021/acs.iecr.7b00295.
[12] E.C. Evarts, Lithium batteries: to the limits of lithium, Nature 526 (2015) 93–95, https://doi.org/10.1038/526S93a.
[13] K. Zaghib, F. Brochu, A. Guerfi, K. Kinoshita, Effect of particle size on lithium intercalation rates in natural graphite, J. Power Sources 103 (2001) 140–146.
[14] L. Yan, G. Chen, S. Sarker, S. Richins, H. Wang, W. Xu, X. Rui, H. Luo, Ultrafine Nb2O5 nanocrystal coating on reduced graphene oxide as anode material for high performance sodium ion battery, ACS Appl. Mater. Interfaces 8 (2016) 22213–22219, https://doi.org/10.1021/acsami.6b06516.
[15] D. Larcher, C. Masquelier, D. Bonnin, Y. Chabre, V. Masson, Effect of particle size on lithium intercalation into a-Fe2O3, J. Electrochem. Soc. 150 (2003) A133–A139, https://doi.org/10.1149/1.1528941.
[16] W. Li, Z. Yang, M. Li, Y. Jiang, X. Wei, X. Zhong, L. Gu, Y. Yu, Amorphous red phosphorus embedded in highly ordered mesoporous carbon with superior lithium and sodium storage capacity, Nano Lett. 16 (2016) 1546–1553, https://doi.org/10.1021/acs.nanolett.5b03903.
[17] K.H. Seng, M.H. Park, Z.P. Guo, H.K. Liu, J. Cho, Catalytic role of Ge in highly reversible GeO 2/Ge/C nanocomposite anode material for lithium batteries, Nano Lett. 1236 (2013) 2–8, https://doi.org/10.1021/nl304716e.
[18] D.H. Youn, N.A. Patterson, H. Park, A. Heller, C.B. Mullins, Facile synthesis of Ge/N-doped carbon spheres with varying nitrogen content for lithium ion battery anodes, ACS Appl. Mater. Interfaces 8 (2016) 27788–27794, https://doi.org/10.1021/acsami.6b09857.
[19] F.M. Xiao, G.G. Peng, Y. Wang, R.H. Tang, Z.P. Xiao, T. Sun, Study on preparation of Si/C anode material by spray dying and carbonization, Mater. Sci. Forum 852 (2016) 928–934. www.scientific.net/MSF.852.928.
[20] A. Mauger, H. Xie, C.M. Julien, Composite anodes for lithium-ion batteries: status and trends, AIMS Mater. Sci. 3 (2016) 1054–1106, https://doi.org/10.3934/matersci.2016.3.1054.
[21] K. Kim, R.A. Adams, P.J. Kim, A. Arora, E. Martinez, J.P. Youngblood, V.G. Pol, Li-ion storage in an amorphous, solid, spheroidal carbon anode produced by dry-autoclaving of coffee oil, Carbon N. Y. 133 (2018) 62–68, https://doi.org/10.1016/j.carbon.2018.03.013.
[22] S. Zou, X. Xu, Y. Zhu, C. Cao, Microwave-assisted preparation of hollow porous carbon spheres and as anode of lithium-ion batteries, Microporous Mesoporous Mater. 251 (2017) 114–121, https://doi.org/10.1016/j.micromeso.2017.05.062.
[23] A. Yu, H.W. Park, A. Davies, D.C. Higgins, Z. Chen, X. Xiao, Free-standing layer-by-layer hybrid thin film of graphene-MnO2 nanotube as anode for lithium ion batteries, J. Phys. Chem. Lett. 2 (2011) 1855–1860, https://doi.org/10.1021/jz200836h.
[24] Z. Zhang, X. Yang, Y. Fu, K. Du, Ultrathin molybdenum diselenide nanosheets anchored on multi-walled carbon nanotubes as anode composites for high performance sodium-ion batteries, J. Power Sources 296 (2015) 2–9, https://doi.org/10.1016/j.jpowsour.2015.07.008.
[25] H. Wang, T. Maiyalagan, X. Wang, Review on recent progress in nitrogen-doped graphene: synthesis, characterization, and its potential applications, ACS Catal. 2 (2012) 781–794.
[26] X.L. Ma, G.Q. Ning, C.L. Qi, C.G. Xu, J.S. Gao, Phosphorus and nitrogen dual-doped few-layered porous graphene: a high-performance anode material for lithium-ion batteries, ACS Appl. Mater. Interfaces 6 (2014) 14415–14422, https://doi.org/10.1021/Am503692g.
[27] C. Chen, P. Hu, X. Hu, Y. Mei, Y. Huang, Bismuth oxyiodide nanosheets: a novel high-energy anode material for lithium-ion batteries, Chem. Commun. 51 (2015) 2798–2801, https://doi.org/10.1039/c4cc09715g.
[28] D. Chen, J.H. Wang, T.F. Chou, B. Zhao, M.A. El-Sayed, M. Liu, Unraveling the nature of anomalously fast energy storage in T-Nb2O5, J. Am. Chem. Soc. 139 (2017) 7071–7081, https://doi.org/10.1021/jacs.7b03141.
[29] C.-M. Park, J.-H. Kim, H. Kim, H.-J. Sohn, Li-alloy based anode materials for Li secondary batteries, Chem. Soc. Rev. 39 (2010) 3115–3141, https://doi.org/10.1039/b919877f.
[30] M.-R. Gao, Y.-F. Xu, J. Jiang, S.-H. Yu, Nanostructured metal chalcogenides: synthesis, modification, and applications in energy conversion and storage devices, Chem. Soc. Rev. 42 (2013) 2986–3017, https://doi.org/10.1039/c2cs35310e.
[31] J. He, Y. Wei, T. Zhai, H. Li, Antimony-based materials as promising anodes for rechargeable lithium-ion and sodium-ion batteries, Mater. Chem. Front. 2 (2018) 437–455, https://doi.org/10.1039/C7QM00480J.
[32] X. Yang, Z. Zhang, Carbon-coated vanadium selenide as anode for lithium-ion batteries and sodium-ion batteries with enhanced electrochemical performance, Mater. Lett. 189 (2017) 152–155, https://doi.org/10.1016/j.matlet.2016.12.001.
[33] D. Lee, C. Park, Tin selenides with layered crystal structures for Li-ion Batteries : interesting phase change mechanisms and outstanding electrochemical behaviors, ACS Appl. Mater. Interfaces 9 (2017) 15439–15448, https://doi.org/10.1021/acsami.7b01829.
[34] H. Kim, Y. Son, J. Lee, M. Lee, S. Park, J. Cho, H.C. Choi, Nanocomb architecture design using germanium selenide as high- performance lithium storage material, Chem. Mater. 28 (2016) 6146–6151, https://doi.org/10.1021/acs.chemmater.6b02016.
[35] X. Wang, H. Wang, Q. Li, H. Li, J. Xu, G. Zhao, H. Li, P. Guo, S. Li, Y. Sun, Antimony selenide nanorods decorated on reduced graphene oxide with excellent electrochemical properties for Li-ion, Batteries 164 (2017) 2922–2929, https://doi.org/10.1149/2.0201713jes.
[36] J. Feng, Q. Li, H. Wang, M. Zhang, X. Yang, R. Yuan, Y. Chai, Hexagonal prism structured MnSe stabilized by nitrogen-doped carbon for high performance lithium ion batteries, J. Alloy. Comp. 789 (2019) 451–459, https://doi.org/10.1016/j.jallcom.2019.03.081.
[37] Y. Idota, T. Kubota, A. Matsufuji, Y. Maekawa, T. Miyasaka, Tin-based amorphous oxide: a high-capacity lithium-lon-storage material, Science 80 (276) (2011) 1395–1397.
[38] A. Hayashi, M. Nakai, H. Morimoto, T. Minami, M. Tatsumisago, Mechanochemical synthesis of SnO-B2O3 glassy anode materials for rechargeable lithium batteries, J. Mater. Sci. 39 (2004) 5361–5364.
[39] T. Minami, A. Hayashi, M. Tatsumisago, Recent progress of glass and glass-ceramics as solid electrolytes for lithium secondary batteries, Solid State Ion. 177 (2006) 2715–2720, https://doi.org/10.1016/j.ssi.2006.07.017.
[40] N. Aotani, K. Iwamoto, S. Kondo, Solid state lithium battery with oxysulfide glass, Solid State Ion. 86–88 (1996) 877–882.
[41] A. Hayashi, T. Konishi, K. Tadanaga, T. Minami, M. Tatsumisago, All-solid-state rechargeable lithium batteries using SnX-P2X5 (X = S and O) amorphous negative electrodes, Res. Chem. Intermed. 32 (2006) 497–506.
[42] A. Hayashi, T. Fukuda, S. Hama, H. Yamashita, H. Morimoto, Lithium ion conducting glasses and glass ¬ ceramics in the systems Li2S-MxSy (M = Al , Si and P) prepared by mechanical milling, J. Ceram. Soc. Jpn. 112 (2004) 695–699.
[43] P. Canepa, G. Sai Gautam, D.C. Hannah, R. Malik, M. Liu, K.G. Gallagher, K. A. Persson, G. Ceder, Odyssey of multivalent cathode materials: open questions and future challenges, Chem. Rev. 117 (2017) 4287–4341, https://doi.org/10.1021/acs.chemrev.6b00614.
[44] M. Sawicki, L.L. Shaw, Advances and challenges of sodium ion batteries as post lithium ion batteries, RSC Adv. 5 (2015) 53129–53154, https://doi.org/10.1039/C5RA08321D.

[45] L. Shi, T. Zhao, Recent advances in inorganic 2D materials and their applications in lithium and sodium batteries, J. Mater. Chem. A. 5 (2017) 3735–3758, https://doi.org/10.1039/C6TA09831B.
[46] A. Zakery, S.R. Elliott, Optical properties and applications of chalcogenide glasses : a review, J. Non-Cryst. Solids 330 (2003) 1–12, https://doi.org/10.1016/j.jnoncrysol.2003.08.064.
[47] J. Hwang, C. Jo, M.G. Kim, J. Chun, E. Lim, S. Kim, S. Jeong, Y. Kim, J. Lee, Mesoporous Ge/GeO_2/carbon lithium-ion battery anodes with high capacity and high reversibility, ACS Nano 9 (2015) 5299–5309, https://doi.org/10.1021/acsnano.5b00817.
[48] Y. Zhao, A. Manthiram, High-capacity, high-rate Bi-Sb alloy anodes for lithium-ion and sodium-ion batteries, Chem. Mater. 27 (2015) 3096–3101, https://doi.org/10.1021/acs.chemmater.5b00616.
[49] H. Lv, R. Chen, X. Wang, Y. Hu, Y. Wang, T. Chen, L. Ma, G. Zhu, J. Liang, Z. Tie, J. Liu, Z. Jin, High-performance Li-Se batteries enabled by selenium storage in bottom-up synthesized nitrogen-doped carbon scaffolds, ACS Appl. Mater. Interfaces 9 (2017) 25232–25238, https://doi.org/10.1021/acsami.7b04321.
[50] G. Kresse, J. Furthmu, Efficient iterative schemes for ab initio total-energy calculations using a plane-wave basis set, Phys. Rev. B. 54 (1996) 11169–11186.
[51] J.P. Perdew, K. Burke, M. Ernzerhof, Generalized gradient approximation made simple, Phys. Rev. Lett. 77 (1996) 3865–3868.
[52] P.E. Blochl, Projector argumented-wave method, Phys. Rev. B. 50 (1994) 17953–17979.
[53] Z. Sun, J. Zhou, Y. Pan, Z. Song, H. Mao, R. Ahuja, Pressure-induced reversible amorphization and an amorphous – amorphous transition in Ge 2 Sb 2 Te 5 phase-change memory material, Proc. Natl. Acad. Sci. 108 (2011) 10410–10414, https://doi.org/10.1073/pnas.1107464108.
[54] J. Liu, D. Lan, X. Huang, F. Zhang, A. Huang, Y. Xiao, Z. Zhao, L. Liu, X. Ke, Z. Shi, Z. Guo, GO@Se@Ni cathode materials for lithium-selenium battery, J. Electrochem. Soc. 166 (2019) 5259–5264, https://doi.org/10.1149/2.0411903jes.
[55] H.S. Im, Y.R. Lim, Y.J. Cho, J. Park, E.H. Cha, H.S. Kang, Germanium and tin selenide nanocrystals for high-capacity lithium ion batteries: comparative phase conversion of germanium and tin, J. Phys. Chem. C 118 (2014) 21884–21888, https://doi.org/10.1021/jp507337c.
[56] M. He, K. Kravchyk, M. Walter, M.V. Kovalenko, Monodisperse antimony nanocrystals for high-rate li-ion and na-ion battery anodes: nano versus bulk, Nano Lett. 14 (2014) 1255–1262, https://doi.org/10.1021/nl404165c.
[57] Y. Li, M.A. Trujillo, E. Fu, B. Patterson, L. Fei, Y. Xu, S. Deng, S. Smirnov, H. Luo, Bismuth oxide: a new lithium-ion battery anode, J. Mater. Chem. A. 1 (2013) 12123–12127, https://doi.org/10.1039/c3ta12655b.
[58] C.C. Nguyen, T. Yoon, D.M. Seo, P. Guduru, B.L. Lucht, Systematic investigation of binders for silicon anodes: interactions of binder with silicon particles and electrolytes and effects of binders on solid electrolyte interphase formation, ACS Appl. Mater. Interfaces 8 (2016) 12211–12220, https://doi.org/10.1021/acsami.6b03357.

Dr. Jassiel Rodriguez is currently a postdoctoral researcher in ViPER group at Davidson School of Chemical Engineering, Purdue University. He received his master and doctoral degrees in materials science and engineering from Nanoscience and Nanotechnology Center at National Autonomous University of Mexico. Dr. Rodriguez's expertise is in the fields of material science, energy storage and electrochemistry. His research is mainly focused on the development of Li- and Na-host active materials with long cycle stability and high specific capacity with potential application in secondary batteries.

Dr. Zhimin Qi received his Bachelor's degree from Zhejiang University of Technology in 2015 and his Ph.D. under the supervision of Prof. Haiyan Wang at Purdue University in 2019. His current research interest mainly focuses on the thin film lithium ion batteries.

Professor Haiyan Wang is the Basil S. Turner Professor of Engineering with a joint appointment between the Schools of Materials Engineering and Electrical and Computer Engineering. Professor Wang's expertise is in electronic ceramic materials and covers processing and characterization of oxide- and nitride-based thin films in nanocomposite form for microelectronics, photonics, optoelectronics, ferroelectric and multiferroics, superconductors, solid oxide fuel cells, and batteries. She has published more than 490 journal papers (total citation over 16500, H-Factor 62), and is a Fellow of ASM International, ACerS, AAAS, APS and MRS.

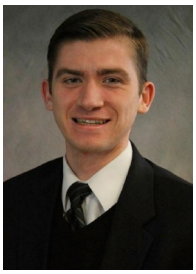

Dr. Mikhail Y. Shalaginov is currently a Postdoctoral Associate at Massachusetts Institute of Technology in the department of Materials Science & Engineering, working in the Photonics Materials research group of Prof. Juejun Hu. His research is focused on developing dynamic meta-optics devices based on phase-change materials for multi-functional imaging and sensing applications in the mid-infrared spectrum. Dr. Shalaginov's research interests include photonic materials, meta-optical systems, quantum optics, integrated photonics, nanophotonics and plasmonics. He is a member of MRS, IEEE, APS, and a co-founder of OSA Purdue Student Chapter, a founder of SPIE Purdue Student Chapter.

Dr. Claudia Gonçalves is currently a postdoctorate researcher of Glass Processing and Characterization Laboratory (GPCL) and Optical Ceramics (OC) at CREOL/College of Optics and Photonics at the University of Central Florida. Her research is focused in the synthesis and characterization of novel glass, glass ceramic and ceramics materials, examining the role of structure/property relationships on resulting optical function and performance. This research is related to optical applications as photosensitive infrared materials, integrated MIR Planar sensors, optics manufacturing science, mid-infrared optical metrology.

Dr. Myungkoo Kang is currently a research scientist in CREOL, the College of Optics and Photonics at the University of Central Florida. Prior to joining UCF, he earned his Ph.D in materials science and engineering at the University of Michigan and worked as a postdoctoral research fellow in the Department of Electrical Engineering at the Pennsylvania State University. His research has focuses on the utilization of spatially-controlled irradiation processes on chalcogenide glasses and III-V compound semiconductors to create novel nanocomposites with spatially-tunable microstructure and desirable properties for next generation gradient refractive index lenses, optical phase-change materials, and plasmonic devices.

Dr. Kathleen Richardson is currently Pegasus Professor of Optics and Materials Science and Engineering at CREOL/College of Optics and Photonics at the University of Central FL, where she runs the Glass Processing and Characterization Laboratory (GPCL). In 2018, she was appointed a Florida Photonics Center of Excellence (FPCE) professor for her ongoing commitments to education and research supporting industry. Prof. Richardson and her research team carry out synthesis and characterization of novel glass and glass ceramic materials for optical applications, examining the role of structure/property relationships on resulting optical function and performance in bulk, planar and fiber optical materials.

Dr. Jonathan Guerrero-Sanchez is an Associate Professor in the Nanoscience and Nanotechnology Center (CNyN) at the National Autonomous University of Mexico (UNAM), where he is working since 2018. His main research interests are in describing the chemical and physical processes on surfaces, interfaces, and nanostructures through computational simulations. He received a B.E. in Materials Science from the BUAP, his M.Sc., and D.Sc. in Materials Science from the Physics Institute of the BUAP. He earned a postdoctoral position at the CNyN-UNAM in 2016, studying the stability and atomic arrangements on magnetic interfaces.

Dr. Maria Guadalupe Moreno-Armenta received her Ph.D. in materials physics from the Center for Science Investigation and Superior Education at Ensenada, Mexico (CICESE) in 2000. After a postdoctoral year at San Diego State University (California) in the field of computational chemistry she has been doing research at Nanoscience and Nanotechnology Center at National Autonomous University of Mexico, interested in the density-functional methods applied to chemistry, solid state physics, surface and materials science. She is focused on first principles calculations of the electronic structure of bulk, surfaces and 2D materials. Her main concern is to propose materials that suggest technological applications.

Prof. Vilas G. Pol is Associate Professor at Purdue University's School of Chemical Engineering. Pol has 19 years of research experience in the fields of energy storage, battery safety, materials chemistry and electrochemistry. He has authored or co-authored more than 180 research publications (h index 44) and an inventor on 25 US patents/applications. Pol is named as '2018 Purdue Faculty Scholar' and is a new GUINNESS WORLD RECORD holder for the fastest time to arrange all the elements of the periodic table. In 2019, he received 'Richard M. Fulrath award' from American Ceramic Society, Professional Achievement Award from AIChE and 'Salutes to Excellence' from American Chemical Society.